Biochimica et Biophysica Acta, 799 (1984) 9–19
Elsevier

BBA 21736

KINETICS AND MECHANISM OF Ca^{2+} BINDING TO ARSENAZO III AND ANTIPYRYLAZO III

PETER L. DOROGI *

Biophysical Laboratory, Department of Physiology and Biophysics, Harvard Medical School, 25 Shattuck Street, Boston, MA 02115 (U.S.A.)

(Received October 17th, 1983)

Key words: Ca^{2+} binding; Arsenazo III; Antipyrylazo III

Equilibrium and temperature-jump spectrophotometric measurements were carried out on arsenazo III (Ar) and antipyrylazo III (Ap) in order to establish the kinetic reaction schemes for complexing of these dyes with Ca^{2+}. The reaction media contained 30 mM Na_2HPO_4 as the buffer salt, at pH 7.4. Dependence of the relaxation rate of arsenazo III on dye and Ca^{2+} concentrations indicates the presence of both CaAr and $CaAr_2$ complexes, with the $CaAr_2$ form being responsible for the slow, 10–20 ms relaxation of this dye. For antipyrylazo III, the relaxation rate is much faster, < 1 ms, and the complexing kinetics can be covered with only a CaAp complex. Unlike arsenazo III, antipyrylazo III binding with Ca^{2+} is rate-limited by a slow structural transition in the dye, taking antipyrylazo III from a low- to a high-affinity structure for Ca^{2+}.

Introduction

Descriptions of calcium-binding to dyes which are useful for spectrophotometric Ca^{2+} measurements are abundant in the literature, and many useful analytical methods have been published for extracting stoichiometry and equilibrium constants of the dye-Ca^{2+} interactions [1–6]. However, biological applications of these dyes often look at transients of absorbance following a stimulus, and equilibrium calibration studies alone are not sufficient for extracting Ca^{2+}-concentration kinetics from the optical signal [7]. The response function for deconvoluting absorbance transients is determined by the kinetic model describing dye-Ca^{2+} interactions. A standard way for establishing the appropriate kinetic model is by observation of the relaxation to a new dye-Ca^{2+} equilibrium after a small shift in an intensive variable, for example, the temperature. The rate of change of each type of dye-Ca^{2+} complex can then be described with a linear first-order differential equation, the solution of which is a linear combination of exponentials. Amplitudes and time constants of these exponentials depend on reactant concentrations, and the concentration dependences can be used to establish the chemical model which underlies the relaxation [8–10].

The present article describes the response of arsenazo III-Ca^{2+} and antipyrylazo III-Ca^{2+} systems to temperature-jumps of 4°C applied to pH-buffered solutions at 21°C. Because protons, Na^+, K^+ and Mg^{2+} ions compete for Ca^{2+} binding sites in ways too complicated to be explained solely by ionic strength effects [11–13], the only ions present in the reaction mixtures were those contributed by the dye salt, added Ca^{2+} and 30 mM Na_2HPO_4 buffer. Relatively simple kinetic models cover equilibrium and kinetic properties of dye relaxation under these conditions. Although numerical values of the various parameters are expected to be different in biological solutions, these results provide a starting framework for

* Present address: Gillette Research Institute, 1413 Research Boulevard, Rockville, MD 20850, U.S.A.

calibration of dye-Ca^{2+} transients measured in situ.

Materials and Methods

Arsenazo III and antipyrylazo III were purchased at the highest purity grade available (Sigma, St. Louis, MO). Purity of the commercial preparations was checked by thin-layer chromatography on Silica Gel G in 3 : 1 volume ratio chloroform/methanol mixture, and the dyes were always found to be 95–98% pure. Stock dye solutions were made up on the day of the experiment by dissolving dye crystals in deionized water containing less than 0.075 ppb Ca^{2+} ions (purification: Hydro Service & Supplies, Durham, NC) and 30 mM Na_2HPO_4 (Sigma, reagent grade) as pH buffer; all solutions were brought to pH 7.4 with 1 N phosphoric acid. Absorbance changes due to dye-Ca^{2+} binding were found to be identical to those measured in the presence of 50 mM Hepes buffer, which agrees with previous findings that phosphate does not interfere with analysis for Ca^{2+} [14,15], and that the Ca^{2+} and pH dependence of absorbance changes in arsenazo III are the same in phosphate and Mops buffer [12]. Addition of 1 mM EGTA to solutions without added Ca^{2+} did not change the absorbance at Ca^{2+}-sensitive wavelengths, indicating that total Ca^{2+} contamination was negligible.

Equilibrium spectra were measured with a Cary 210 (Varian, Palo Alto, CA) spectrophotometer. Temperature-jump studies were carried out with an apparatus described previously [16]. The instrument produces a 4 °C temperature increase within 10 μs by discharging a 0.1 μF capacitor, charged to 15 000 V, across a 0.8 ml quartz measuring cell. Data were recorded on a Biomation (Cupertino, CA) 805 waveform recorder, and transferred to a PDP 11/34 computer for storage and analysis.

All glassware, including the measuring cells, were washed with 10 mM EGTA/10 mM EDTA solution and rinsed with deionized water.

Analysis and Results

General considerations

Arsenazo III (Ar) is attractive for biological studies because it undergoes a large spectral change upon binding Ca^{2+} and because it has a micromolar dissociation constant with Ca^{2+}; the structure of this dye is shown in Fig. 1a. At physiological pH, arsenazo III is thirty times more sensitive to H^+ than to Ca^{2+} binding, and the dye releases a proton upon binding Ca^{2+} [15]. A change in pH produces an apparent change in the K_D for Ca^{2+}, and a change in dye absorbance due to inadequate pH buffering can be erroneously interpreted as a change in Ca^{2+} concentration [12]. In solution, arsenazo III can take several different protonated states, and the molar absorptivities of these species differ at any pH [11,14]. Arsenazo III forms both 1 : 1 and 2 : 1 Ar : Ca^{2+} complexes under some ionic conditions [17–19], and this multiple stoichiometry complicates analysis of dye signals.

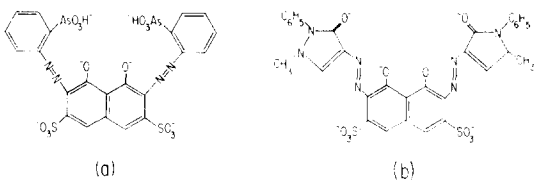

Fig. 1. Structural diagrams of (a) arsenazo III and (b) antipyrylazo III.

It has been suggested that the sensitivity of dye absorbance in the 650–660 nm range reflects involvement of the peri-dioxy groups in Ca^{2+} chelation [12]: deprotonation of the hydroxyls transfers the dye to a quinone-like form, with the electronegative oxygens stabilizing the association with Ca^{2+}.

Antipyrylazo III (Ap) was used by Budesinsky [20] for Ca^{2+} measurement at high pH, and biological applications were first reported by Scarpa et al. [21]; the structure of antipyrylazo III is shown in Fig. 1b. This dye can be used for Ca^{2+} measurement in the 10–1000 μM range, but Ca^{2+} affinity and Ca^{2+}-induced spectral changes are very sensitive to ionic conditions. Like arsenazo III, antipyrylazo III is also an acid-base indicator, and biological calibration of dye absorbance properties should be done in situ, using the dual-wavelength method which subtracts absorbance changes not specific to Ca^{2+} [21]. Multiple Ap : Ca^{2+} stoichiometric forms have been reported under certain reaction conditions [22–24].

Equilibrium titrations: arsenazo III

In 30 mM Na_2HPO_4 buffer at pH 7.4, Ca^{2+} binding causes a large absorbance increase, ΔA, in arsenazo III at 650 nm. Equilibrium Ca^{2+}-titrations of this dye can be analyzed for the simultaneous presence of both 1:1 and 2:1 dye-Ca^{2+} complexes using the analysis detailed in Refs. 6 and 25. In brief, conservation conditions on total dye and calcium, $[Ar_T]$ and $[Ca_T]$, allow writing of the dissociation constant, K_1, for the 1:1 complex, CaAr, in the form

$$K_1 = ([Ca_T] - \Delta A/\Delta\epsilon_1)([Ar_T] - \Delta A/\Delta\epsilon_1)\Delta\epsilon_1/\Delta A, \quad (1)$$

where $\Delta\epsilon_1$ is the molar difference extinction coefficient due to Ca^{2+} binding,

$$\Delta\epsilon_1 = \epsilon_{CaAr} - \epsilon_{Ar}, \quad (2)$$

at 650 nm. If the correct value of $\Delta\epsilon_1$ is inserted into Eqn. 1 and only 1:1 complexes are stable, each titration data point ($[Ar_T]$, $[Ca_T]$, ΔA) must predict the same value for K_1, because this quantity is the same for all reactant concentrations (K_1 will vary with ionic strength, but the large excess of buffer ions in the present case renders the ionic strength correction the same for each titration point). The optimal value of $\Delta\epsilon_1$ can be established with a computerized trial method. Fig. 2a shows that the 1:1 binding model is inadequate: $\Delta\epsilon_1$ was set at the value which best satisfied the K_1-constancy condition for two similar $[Ar_T]$ conditions, 25 and 29 μM. Predicted values of K_1 are shown as circles and triangles in Fig. 2a. When the same value of $\Delta\epsilon_1$ was used for titration data measured with a much higher dye concentration, $[Ar_T] = 50$ μM, significantly different K_1 values are predicted by Eqn. 1, demonstrating inconsistency of the 1:1 binding model; the latter K_1 values are shown as squares in Fig. 2a.

Prediction of lower K_1 values at high $[Ar_T]$ can be interpreted physically to suggest that Ca^{2+} ions can interact with more than one dye molecule, because the chance of forming $CaAr_2$ complexes would be greater at higher dye concentrations. Using the method of Ref. 6 for the case where both 1:1 and 2:1 dye-Ca^{2+} complexes are present, all parameters, K_1, $\Delta\epsilon_1$, K_2 and $\Delta\epsilon_2$, can be determined. Estimates are obtained for K_1 and $\Delta\epsilon_1$

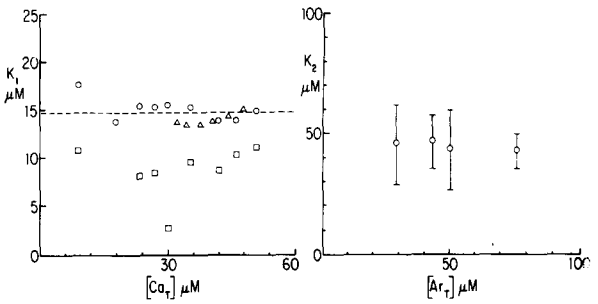

Fig. 2. (a) Calculated values of K_1, from Eqn. 1, for three Ca^{2+}-titrations of arsenazo III with $[Ar_T] = 25$ μM (○), 29 μM (△) and 50 μM (□). (b) Means and standard deviations of K_2 values calculated with Eqn. 5, showing constancy with $[Ar_T]$.

from titrations with low $[Ar_T]$, and are used as initial estimates to calculate K_2 with only $\Delta\epsilon_2$ as free parameter. Defining

$$K_2 = [CaAr][Ar]/[CaAr_2], \quad (3)$$

$$\Delta\epsilon_2 = \epsilon_{CaAr_2}/2 - \epsilon_{Ar}, \quad (4)$$

mass conservation conditions on dye and calcium, and the definition $K_1 = [Ca][Ar]/[CaAr]$ allow expression of K_2 in terms of one variable, $\Delta\epsilon_2$:

$$K_2 = 2\Delta\epsilon_2[Ca][Ar]^2/(\Delta A K_1 - [Ca][Ar]\Delta\epsilon_1), \quad (5)$$

where [Ca] and [Ar] denote concentrations of unbound reactants, and

$$[Ca] = K_1(2[Ca_T]\Delta\epsilon_2 - \Delta A)/\{2\Delta\epsilon_2 K_1 + [Ar](2\Delta\epsilon_2 - \Delta\epsilon_1)\}$$

$$[Ar] = -D/2 + (D^2 - 4C)^{1/2}/2$$

$$D = \{K_1 + (1 - \Delta\epsilon_1/\Delta\epsilon_2)([Ca_T] - \Delta A/(2\Delta\epsilon_2))\}$$
$$/\{1 - \Delta\epsilon_1/(2\Delta\epsilon_2)\} + \Delta A/\Delta\epsilon_2 - [Ar_T]$$

$$C = -K_1([Ar_T] - \Delta A/\Delta\epsilon_2)/\{1 - \Delta\epsilon_1/(2\Delta\epsilon_2)\}.$$

With K_1 and $\Delta\epsilon_1$ determined at low dye concentrations,

$$K_1 = 15\ \mu M,\ \Delta\epsilon_1 = 0.0155\ \mu M^{-1}\cdot cm^{-1},$$

K_2 could be estimated in a consistent fashion with

the choice

$$\Delta\epsilon_2 = 0.0125\ \mu M^{-1}\cdot cm^{-1},$$

which yielded

$$K_2 = 49\ \mu M.$$

The distribution of calculated K_2 values is shown in Fig. 2b for a 25–50 μM range of dye concentrations. The dependence of K_2 on $[Ca_T]$ for each particular $\{Ar_T\}$ was also constant within a small scatter range.

The ability of these parameters to simulate experimental absorbance changes is shown in Fig. 3, where the curves depict behavior of the function

$$\Delta A = \Delta\epsilon_1[CaAr] + 2\Delta\epsilon_2[CaAr_2], \quad (6)$$

with [CaAr] and $[CaAr_2]$ calculated from the determined values of K_1 and K_2.

Equilibrium titrations: antipyrylazo III

Although antipyrylazo III has been reported to form higher-order complexes with calcium under certain ionic conditions, for example, when [Ca] is in the millimolar range [24], absorbance changes measured in 30 mM Na_2HPO_4 pH-buffer are covered with a 1 : 1 complexing model, provided that $\{Ca_T\} \lesssim 1$ mM and $\{Ap_T\} \lesssim 100\ \mu$M. Fig. 4a shows the method of Eqn. 1 applied to Ca^{2+}-titrations at $[Ap_T] = 40$, 50 and 60 μM; the measurement wavelength is 595 nm, where Ca^{2+} can be detected by an absorbance decrease. Optical and binding parameters for the 1 : 1 complex are indicated to be

$$K_1 = 0.48\ \text{mM},\ \Delta\epsilon_1 = -0.0050\ \mu M^{-1}\cdot cm^{-1}.$$

Experimental and theoretical data are compared in Fig. 4b, where curves show the predicted absorbance change as

$$\Delta A = \Delta\epsilon_1[CaAp]. \quad (7)$$

Kinetic mechanism of arsenazo III-Ca^{2+} complexing

Relaxation kinetic studies were carried out to see if absorbance kinetics after a step increase in temperature can be described with the above equilibrium models, and to determine rate constants of kinetically resolvable binding steps.

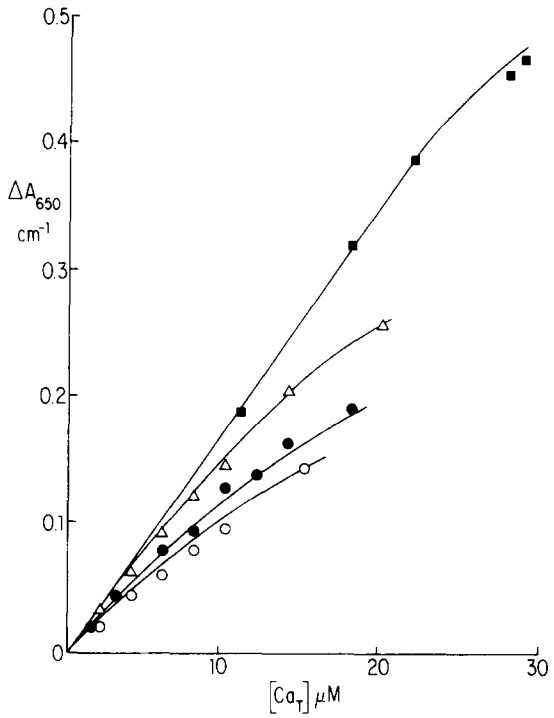

Fig. 3. Comparison of experimental absorbance changes at 650 nm with prediction of Eqn. 6 (curves); $[Ar_T] = 25\ \mu$M (○), 29 μM (●), 43 μM (△) and 75 μM (■).

If both 1 : 1 and 2 : 1 complexes contribute to the arsenazo III-Ca^{2+} interaction, then three types of bimolecular reactions can be presumed to exist:

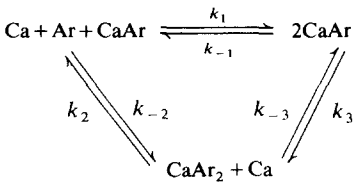

(8)

Because all reactions are reversible, requirement of detailed dynamic balance at equilibrium imposes Eqn. 9,

$$k_1k_2k_3 = k_{-1}k_{-2}k_{-3}, \quad (9)$$

which reduces the total number of relaxation modes for Scheme 8 to only two. The experimental relaxation signal does, in fact, consist of two resolvable modes: there is at least one mode which equi-

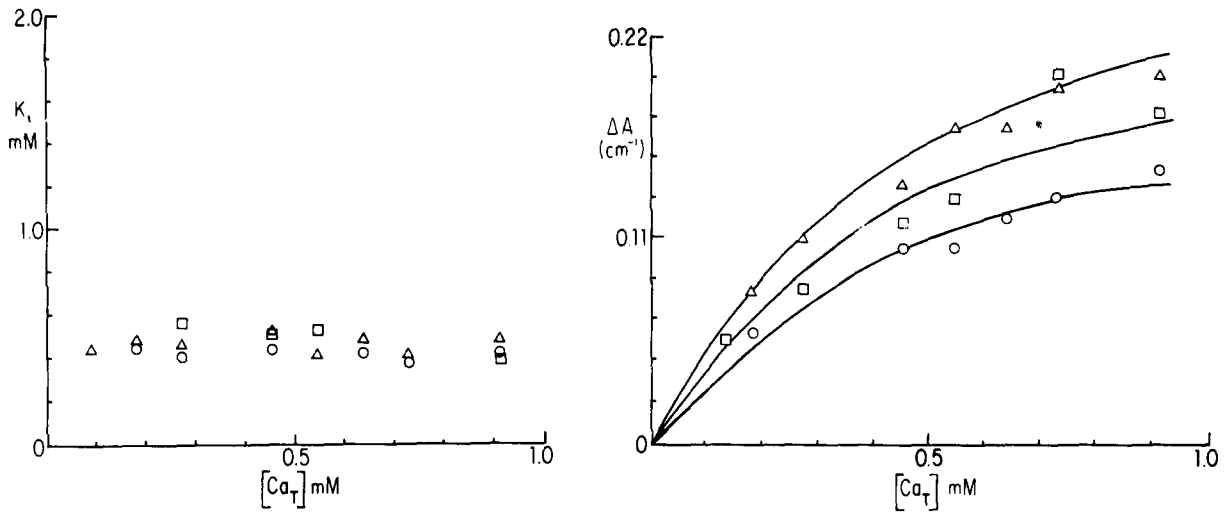

Fig. 4. (a, left). Values of K_1 calculated from absorbance change in antipyrylazo III using eqn. 1 with $\Delta\epsilon_1 = -0.0050\ \mu M^{-1}\cdot cm^{-1}$; $[Ap_T] = 40\ \mu M$ (○), 50 μM (□) and 60 μM (△). (b, right). Comparison of experimental and predicted absorbance changes. Symbols are as in part a, and curves show result of 1:1 complexing model with $\Delta\epsilon_1 = -0.0050\ \mu M^{-1}\cdot cm^{-1}$ and $K_1 = 0.48$ mM.

librates faster than the resolution time of the spectrometer ($\lesssim 10\ \mu s$), whereas the kinetically resolvable signal consists of only one exponential component, which relaxes with a time constant, τ, of about 10 ms. The faster component can be shown to include contributions from Na^+, as well as Ca^{2+} binding to dye, with Na^+-effects being implicit in apparent Ca^{2+} binding parameters [13]. Similarly, the slow relaxation is covered by Scheme 8, with apparent parameters masking competing, rapidly relaxing Na^+-dye reactions.

Fig. 5a and b show amplitudes and time constants of the slow mode for two representative experiments. For the analysis, an interesting feature is that τ does not vary significantly with changing $[Ca_T]$, but does reflect changes in $[Ar_T]$. This suggests that the 1:1 complexing reaction, $Ca + Ar \rightleftharpoons CaAr$, does not affect the rate of the slow mode. Furthermore, sensitivity to $[Ar_T]$ implies that the rate of relaxation is limited by the concentration of free dye, [Ar], reflecting the reaction $Ar + CaAr \rightleftharpoons CaAr_2$ in Scheme 8. Physically, this can be understood if stable association of Ar with CaAr has to overcome large steric (or, more

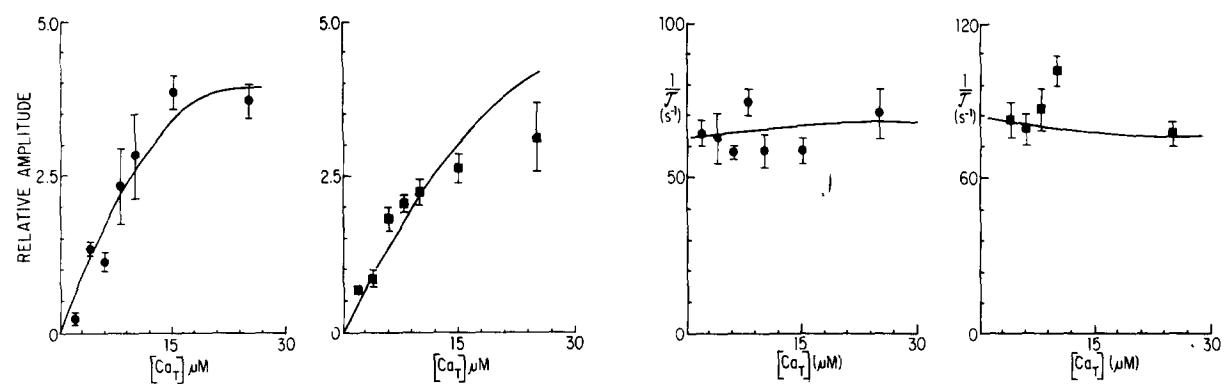

Fig. 5. (a, two left-hand panels). Relaxation amplitudes of optical transients after temperature-jumps are applied to different arsenazo III-Ca^{2+} mixtures; $[Ar_T] = 25\ \mu M$ (●) and 50 μM (■). Curves show relative behavior predicted by Eqns. 15–18. (b, two right-hand panels). Relaxation time constants of arsenazo III-Ca^{2+} slow mode, compared with prediction of Eqn. 13.

simply, electrostatic) barriers since both reactants carry a net negative charge at pH 7.4. In contrast, association of Ca^{2+} and dye should be limited only by competing effects from Na^+ and H^+ ions, and solvation water molecules.

The analysis with Scheme 8 can therefore assume that reaction 1 is rapid, and that its parameters are implicitly dependent on coupled equilibria with other solution components. The slow relaxation reflects coupling of reactions 2 and 3 in Scheme 8, and its expression in terms of rate constants can be reduced to two terms,

$$\frac{1}{\tau} = k_{-2}A + k_{-3}B, \tag{10}$$

where

$$A = 2[\mathrm{CaAr}]\xi(2K_1 + [\mathrm{Ar}]) + [\mathrm{Ar}]^2 K_1^{-1}\xi(K_1 - [\mathrm{Ca}]) + K_2, \tag{11}$$

$$B = 2[\mathrm{Ca}][\mathrm{CaAr}]K_2^{-1}\xi(2K_1 + [\mathrm{Ar}]) + [\mathrm{CaAr_2}]\xi(K_1 - [\mathrm{Ca}]) + [\mathrm{Ca}], \tag{12}$$

with $\xi = (K_1 + [\mathrm{Ca}] + [\mathrm{Ar}])^{-1}$, $K_1 = k_{-1}/k_1$ and $K_2 = k_2/k_{-2}$. The latter two quantities are known from equilibrium titrations, allowing calculation of both A and B for each set of reactant concentrations ($[\mathrm{Ar_T}]$, $[\mathrm{Ca_T}]$). Fig. 6 illustrates the trend of A and B with $[\mathrm{Ca_T}]$ for the particular dye concentration $[\mathrm{Ar_T}] = 76\ \mu\mathrm{M}$. In general, for $[\mathrm{Ar_T}] < 100\ \mu\mathrm{M}$ and $[\mathrm{Ca_T}] < 10\ \mu\mathrm{M}$, the condition $A \gg B$ is found, which suggests that the approximation

$$\tau^{-1} \approx k_{-2}A \tag{13}$$

can be used at micromolar calcium concentrations. Fig. 7 shows a plot of $(\tau B)^{-1}$ against A/B, supporting this approximation: the linearity of data in Fig. 7 shows that τ^{-1} is proportional to A. The analogous plot of $(\tau A)^{-1}$ vs. B/A (not shown) does not shown any clear trend, supporting the argument, that at low $[\mathrm{Ca_T}]$ at least, measured values of τ are not significantly correlated with variation in the quantity B. Slope and intercept of the fitted regression line in Fig. 7 give $k_{-2} = 0.95\ \mu\mathrm{M}^{-1}\cdot\mathrm{s}^{-1}$, and suggest that $k_{-3} \ll k_{-2}$. The curves in Fig. 5a show predictions of Eqn. 13 with the determined values of K_1, K_2 and k_{-2} ($k_2 = K_2 k_{-2} = 46.6\ \mathrm{s}^{-1}$).

The amplitude of relaxation, ΔA induced by the temperature-jump, depends upon the sign and magnitude of the enthalpic changes, ΔH_i, in the two reactions, 1 and 2. This connection is established via the van't Hoff law, $\delta K/K = (\Delta H/RT^2)\delta T$ [10], which relates the change, δK, produced in the equilibrium constant of each reaction to the imposed temperature change, δT; R is the gas constant. If the total absorbance change due to

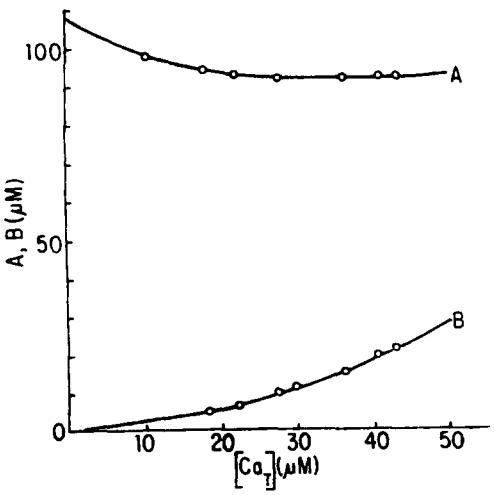

Fig. 6. Relative magnitudes of coefficients A and B, reflecting relative importance of reactions 2 and 3 in Scheme 8 for the slow-mode time constant. Total dye concentration = 76 μM.

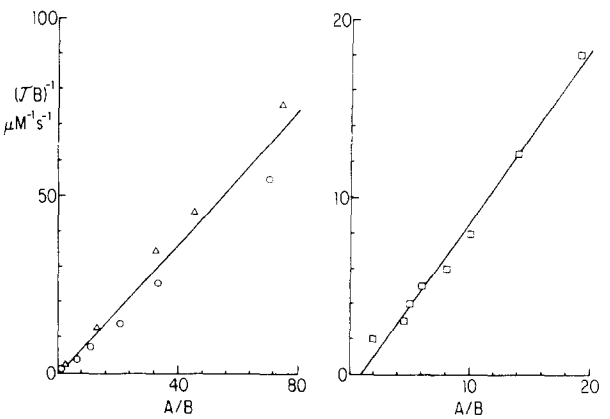

Fig. 7. Plot of Eqn. 10 in the form $(\tau B)^{-1} = k_{-2}(A/B) + k_{-3}$ for $[\mathrm{Ar_T}] = 25\ \mu\mathrm{M}$ (○), 50 μM (△) and 75 μM (□), with fitted regression lines. Linear trend supports correctness of Scheme 8.

δT is written as $\delta(\Delta A)$, for arsenazo III this quantity is the sum of two terms,

$$\delta(\Delta A) = \Delta\epsilon_1 \delta[\mathrm{CaAr}] + 2\Delta\epsilon_2 \delta[\mathrm{CaAr_2}], \tag{14}$$

where δ[c] defines the change in equilibrium concentration of species c due to the temperature-jump. The van't Hoff law relates $\delta(\Delta A)$ to the association enthalpies of reactions 1 and 2, ΔH_1 and ΔH_2, in Scheme 8:

$$\delta(\Delta A)_s = \frac{\delta T \Delta\epsilon_1}{RT^2}(\Gamma_1 \Delta H_1 + \Gamma_2 \Delta H_2), \tag{15}$$

where $\delta(\Delta A)_s$ is the slow-mode amplitude. The weighting factors Γ_1 and Γ_2 take the form

$$\Gamma_1 = FK_1[\mathrm{CaAr}]([\mathrm{Ar}] - [\mathrm{CaAr}]), \tag{16}$$

$$\Gamma_2 = \left\{ F\xi - ([\mathrm{Ar}] - [\mathrm{CaAr}])^{-1} \right\} K_2[\mathrm{CaAr_2}], \tag{17}$$

where ξ is defined in Eqns. 11 and 12, and

$$F = \left\{ \frac{K_2 + 2[\mathrm{CaAr}]}{[\mathrm{Ar}] - [\mathrm{CaAr}]} + \frac{2\Delta\epsilon_2}{\Delta\epsilon_1} \right\} \times \left\{ K_2(\xi + [\mathrm{CaAr_2}]) + 4K_1[\mathrm{CaAr}] + [\mathrm{Ar}]^2 \right\}^{-1}.$$

Temperature-jump experiments are not a good way to estimate numerical values for ΔH, because reaction enthalpies can vary greatly with temperature, and thermodynamics does not predict the form of this variation. The present approach can nonetheless provide useful information on heat absorption properties of reactions 1 and 2. Fig. 8a

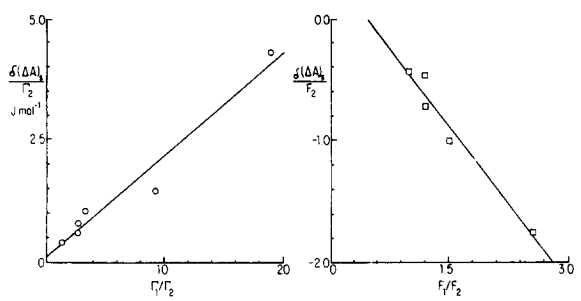

Fig. 8. (a, left). Plot for estimating ΔH_1 and ΔH_2 from slow-mode amplitude, $\delta(\Delta A)_s$, defined in Eqns. 15–17, with $[\mathrm{Ar_T}] = 75\ \mu$M. Slope $= \Delta H_1 \cong 0.20f$ J·mol^{-1}, intercept $= \Delta H_2 \cong 0.14f$ J·mol^{-1}, where f is the absorbance/voltage conversion factor. (b, right). Similar plot for antipyrylazo III for one experiment with $[\mathrm{Ap_T}] = 40\ \mu$M. F_1 and F_2 refer to the factors of ΔK_3 and ΔK_4 in Eqn. 29, with $\Delta K_i/K_i = (\Delta H_i/RT^2)\delta T$. Slope $= \Delta H_3 \cong -0.88g$ J·mol^{-1}, intercept $= \Delta H_4 \cong 0.42g$ J·mol^{-1}, with g as the particular absorbance/voltage conversion factor.

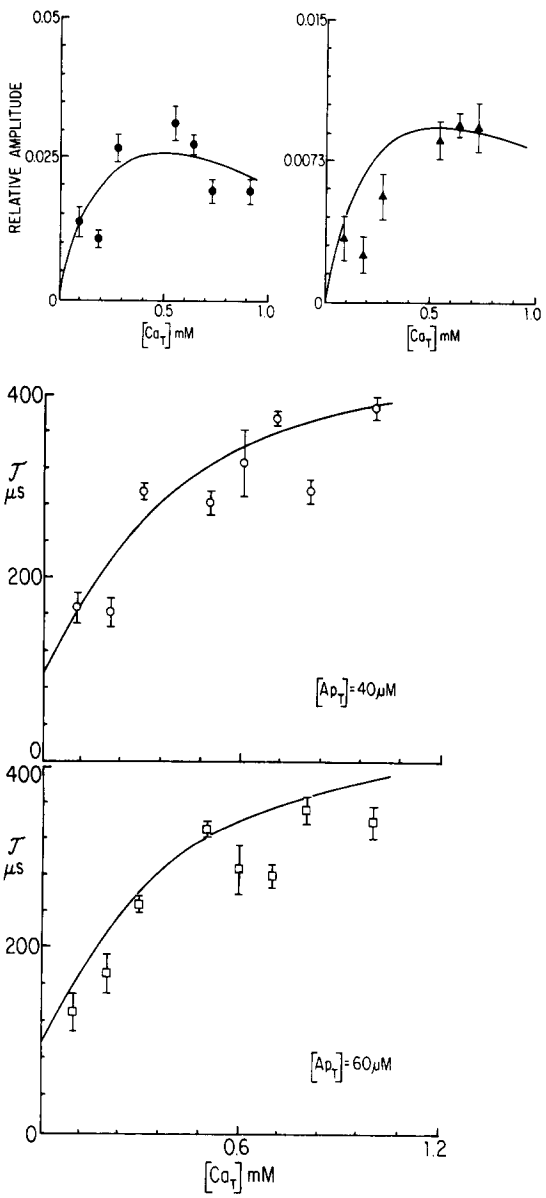

Fig. 9. (a, two upper panels). Comparison of antipyrylazo III-Ca^{2+} relaxation amplitude for different $[\mathrm{Ca_T}]$ values, at $[\mathrm{Ap_T}] = 40\ \mu$M (●) and 60 μM) (▲), with prediction of Eqn. 23 when K_1 is set at 0.48 mM. (b, two lower panels). Comparison of Ap-Ca^{2+} relaxation time constant, τ, for $[\mathrm{Ap_T}] = 40\ \mu$M (○) and 60 μM (□), with prediction of Eqn. 21.

provides a typical plot of $\delta(\Delta A)_s/\Gamma_2$ against Γ_1/Γ_2; the approximate relation

$$\Delta H_1 \approx \Delta H_2 \tag{18}$$

is consistently found. Because absorbance decreases with positive δT, $\delta(\Delta A)_s$ is negative, ΔH_1 and ΔH_2 are negative, showing that enthalpic changes due to CaAr and $CaAr_2$ complexing are both favorable, reducing the free energy of the system. It should be noted, however, that ΔH_1 and ΔH_2 are net changes, with ΔH_1 incorporating reactions due to other solution components and ΔH_2 encompassing several slow structural rearrangements, with similar kinetics, in the $CaAr_2$ complex [13].

The prediction of Eqn. 15, obtained by setting $\Delta H_1 = \Delta H_2$ and scaling for the appropriate electronic/optical conversion, is shown in Fig. 5b for two arsenazo III concentrations, 25 and 50 μM.

Kinetic mechanism of antipyrylazo III-Ca^{2+} complexing

In qualitative agreement with equilibrium studies, relaxation of the Ap-Ca^{2+} system to its new equilibrium after a temperature-jump proceeds as a single kinetic mode. At higher calcium concentrations, $[Ca_T] > 1$ mM, a total of three relaxation modes can be resolved, suggesting a more complicated dye-Ca^{2+} complexing mechanism. The present analysis is limited to the range $[Ap_T] \leqslant 60$ μM, $[Ca_T] \leqslant 1$ mM, wherein only 1 : 1 complexing appears to be stable (in 30 mM Na_2HPO_4 buffer at pH 7.4).

The most noteworthy feature of the Ap-Ca^{2+} relaxation is a clearcut slowing of the relaxation rate as $[Ca_T]$ is raised from zero to low values, with this effect plateauing as $[Ca_T]$ is further increased: Fig. 9a and b show the dependences of relaxation amplitudes and time constants on $[Ca_T]$ for two dye concentrations. The retarding effect of Ca^{2+} on the relaxation rate, τ^{-1}, indicates that the rate of development of the Ca^{2+}-induced absorbance change is not limited by binding of calcium.

The data can be interpreted as described in Ref. 26, with Ca^{2+} binding occurring either by Ca^{2+}-induced or Ca^{2+}-independent isomerization pathways:

$$Ca + Ap \underset{k_{-1}}{\overset{k_1}{\rightleftharpoons}} CaAp \underset{k_{-2}}{\overset{k_2}{\rightleftharpoons}} CaAp' \text{ (induced)}, \tag{19}$$

$$Ca + \underset{k_{-3}\uparrow\downarrow k_3}{\overset{Ap}{Ap'}} \underset{k_{-4}}{\overset{k_4}{\rightleftharpoons}} CaAp' \text{ (isomerization)}. \tag{20}$$

Schemes 19 and 20 display identical equilibrium properties, but can be distinguished by kinetic methods [26]. The experimental relaxation rates are related to Ca^{2+} concentrations as predicted by Scheme 20:

$$\frac{1}{\tau} = k_3 + k_{-3}\frac{[Ap'] + K_4}{[Ca] + [Ap'] + K_4}, \tag{21}$$

where $K_4 = k_{-4}/k_4$.

Expression 21 is representative of the special case where step 3 is slow, i.e., kinetically resolvable, but step 4 is fast. The time constant τ of the relaxation increases with [Ca] if the condition $[Ca] \gtrsim K_4 + [Ap']$ is met. The value of τ at high [Ca] ($\approx [Ca_T]$) is k_3^{-1}; extrapolating the behavior of τ with [Ca] to $[Ca_T] = 0$ gives an estimate for $k_3 + k_{-3}$. Numerical fitting gives the values $k_3 = 1.9$ ms^{-1}, $k_3 + k_{-3} = 11.1$ ms^{-1}; $k_{-3} = 9.2$ ms^{-1}. The overall dissociation equilibrium constant, K_1, determined as in Fig. 4a, is related to the elementary equilibria in Scheme 20 as

$$K_1 = (1 + K_3)K_4, \tag{22}$$

where $K_3 = k_{-3}/k_3 = 4.8$. Inserting the value $K_1 = 0.48$ mM gives $K_4 = 84$ μM. The predictions of Eqn. 21 are shown by the curves in Fig. 9b.

The relaxation amplitude for 1 : 1 complexing is proportional to the quantity Ω, defined as

$$\Omega = \frac{K_1}{2}\left[\frac{\Theta^{-1}}{(\Theta^{-2} - 4[Ca_T][Ap_T])^{1/2}} - 1\right], \tag{23}$$

where $\Theta = [Ca_T] + [Ap_T] + K_1$. The behavior of Ω with $K_1 = 0.48$ mM is shown by the curves in Fig. 9a.

Relative enthalpic changes associated with the two reaction steps in Scheme 20 can be estimated by the graphical method used above for the arsenazo III-Ca^{2+} system. For the Ap-Ca^{2+} sys-

TABLE I

EQUILIBRIUM AND KINETIC CONSTANTS OF ARSENAZO III (Ar) AND ANTIPYRYLAZO III (Ap) INTERACTION WITH CALCIUM AT pH 7.4, $T = 25°C$ IN 30 mM Na_2HPO_4 BUFFER

Mechanism	Parameter values	Reaction enthalpy
Arsenazo III (when $[Ca_T] < 10\ \mu M$)		
$Ca + Ar \underset{\text{(fast)}}{\overset{K_1}{\rightleftharpoons}} CaAr$	$K_1 = 15\ \mu M$	exothermic
$Ar + CaAr \underset{k_2}{\overset{k_{-2}}{\rightleftharpoons}} CaAr_2$	$k_{-2} = 0.95\ \mu M^{-1} \cdot s^{-1}$ $k_2 = 46.6\ s^{-1}$	exothermic
Antipyrylazo III (when $[Ca_T] < 1$ mM)		
$Ap \underset{k_{-3}}{\overset{k_3}{\rightleftharpoons}} Ap'$	$k_3 = 1.9\ ms^{-1}$ $k_{-3} = 9.2\ ms^{-1}$	endothermic
$Ca + Ap' \underset{\text{(fast)}}{\overset{K_4}{\rightleftharpoons}} CaAp'$	$K_4 = 84\ \mu M$	exothermic

tem, $\delta(\Delta A)$ at 595 nm is expressible as

$$\delta(\Delta A) = \epsilon_{Ap'}\delta[Ap'] + \epsilon_{Ap}\delta[Ap] + \epsilon_{CaAp}\delta[CaAp]. \quad (24)$$

Assuming that ΔH_3 is finite, the absence of any absorbance change in the absence of Ca^{2+} suggests that $\epsilon_{Ap'} \approx \epsilon_{Ap}$. Using this relation and mass conservation laws gives the expression of the absorbance change as

$$\delta(\Delta A)_s = -\Delta\epsilon\left[\{K_3\alpha(1+K_4)\}\frac{\Delta K_3}{K_3} + K_4\{\beta(1+K_4)+[Ap]\}\frac{\Delta K_4}{K_4}\right], \quad (25)$$

where $\Delta\epsilon = \epsilon_{CaAp} - \epsilon_{Ap}$. Quantities α and β denote the expressions

$$\alpha = \frac{[CaAp]}{[Ca]+(1+K_4)([Ap]+K_3)},$$

$$\beta = \frac{-[Ap]([Ap]+K_3)}{[Ca]+(1+K_4)([Ap]+K_3)}.$$

The van't Hoff law allows expression of $\delta(\Delta A)_s$ in terms of enthalpy changes (ΔH_3 and ΔH_4: plots such as the one shown in Fig. 8b suggest the approximate relationship $\Delta H_3 \approx -2\Delta H_4$, with ΔH_3 positive. Hence, dye-Ca^{2+} combination produces a net heat loss for both arsenazo III and antipyrylazo III, but the endothermic character of the Ap→Ap′ transition accounts, in part at least, for the greater stability of the low Ca^{2+}-affinity, antipyrylazo III conformation. The reaction parameters for both dyes are summarized in Table I.

Discussion

Arsenazo III and antipyrylazo III have been used widely as determinants of Ca^{2+} concentration in biological systems, but there is still no consensus on the chemical models which describe dye-Ca^{2+} complexing. The disagreements may be due to differences in reaction conditions, or to differences in the theoretical methods used to extract chemical parameters from the spectrophotometric data. By providing rate constants in addition to equilibrium constants, relaxation kinetics permit better discrimination among plausible reaction models than is possible from equilibrium studies alone.

Because one is usually interested in finding the simplest formalism for extracting Ca^{2+}-concentration kinetics from the dye signal, and not in the details of dye chemistry, the reaction models derived here are not necessarily a complete picture of the molecular events. The present studies give clear evidence of $CaAr_2$ complexing, showing that the characteristic slow arsenazo III signal reflects stabilizing rearrangements in this complex. Ionic conditions used here are far less complicated than those of biological fluids, but the present study

should provide guidelines for developing reaction schemes which are suitable for complicated chemical conditions.

A serious drawback in some biological applications is that the dyes bind to cells and cell components. Arsenazo III has been reported to bind extensively to muscle cell components [27] and antipyrylazo III reacts with acetylcholine receptor protein in the presence of calcium [24]. An interesting recent observation in our laboratory is that when a solution of arsenazo III in Ca^{2+}-free phosphate buffer is mixed with a suspension of red cell ghosts, there follows a slow, 5–10 min decrease in dye absorbance at 550 nm, a Ca^{2+} sensitive wavelength, but no optical change can be detected at 650 nm; Ca^{2+} affects the absorbance about equally at 550 and 650 nm under these ionic conditions. Following the suggestion of Ogan and Simons [12] that the sensitivity of dye absorbance at 650 nm may be due to its deprotonated form, the failure to detect a signal with red cell ghosts at 650 nm may indicate that only the protonated form of arsenazo III reacts with the ghosts. The related finding of Baylor et al. [28] that the dichroic component of arsenazo III signals, due to the binding of dye to oriented subcellular structures in frog twitch fibers, is minimal at 660 nm, may also reflect a similar phenomenon. Presence of two chemically different forms of this dye in muscle preparations is suggested by the observation of different time courses in signals monitored at 600 nm compared with that monitored at 660 nm [28], and also by a larger signal at 660 nm than at 600 nm [7]. This difference has also been detected in molluscan neurons [29]. Relaxation experiments carried out at several different wavelengths should allow separate characterization of the different dye forms, and fundamentally different chemical models may need to be derived for arsenazo III at different wavelengths.

Temperature-jump studies carried out in our laboratory on solutions containing the Ca^{2+}-sensitive protein calmodulin, and either arsenazo III or antipyrylazo III, indicate that these dyes can resolve two relaxation modes associated with Ca^{2+} binding to this protein. Both dyes can detect a slow, 5 s, relaxation in calmodulin, reflected as a slow Ca^{2+} release process. In addition, antipyrylazo III can be used to sense a faster process, with a time constant of about 10 ms. These preliminary studies point to the usefulness of these dyes as Ca^{2+} indicators, and the kinetic schemes derived here can be used to interpret the dye signals in terms of equilibrium and rate parameters of the biological components.

Acknowledgements

I am indebted to Dr. Arthur K. Solomon for his continuing support of this project and for his collaboration in many insightful discussions. Purity analysis of the dyes was carried out with the helpful guidance of Dr. Michael F. Lukacovic, and the temperature-jump apparatus used in these studies was designed by Dr. Alfred A. Pandiscio and constructed by Mr. Bernard Corrow. This work was carried out under the tenure of a Fellowship Award from the Massachusetts Affiliate of the American Heart Association, Award Number 13-404-823, and was supported by grants from the National Institutes of Health, Grant 5-RO1-HL14820, and the National Science Foundation, Grant PCM-78-22577, awarded to Dr. Solomon.

References

1 Durham, A.C.H. and Walton, J.M. (1983) Cell Calcium 4, 47–55
2 Ohnishi, S.T. (1979) Biochim. Biophys. Acta 586, 217–230
3 Thomas, M.V. (1979) Biophys. J. 25, 541–548
4 Ahmed, Z., Kragie, L. and Connor, J.A. (1980) Biophys. J. 32, 907–920
5 Bauer, P.J. (1981) Anal. Biochem. 110, 61–72
6 Dorogi, P.L. and Neumann, E. (1981) Biophys. Chem. 13, 117–123
7 Palade, P. and Vergera, J. (1982) J. Gen. Physiol. 79, 679–707
8 Eigen, M. and DeMaeyer, L. (1963) in Technique of Organic Chemistry (Weissberger, A., ed.) Vol. III, Ch. 2, Wiley, New York
9 Czerlinski, G.H. (1966) Chemical Relaxation, Marcel Dekker, New York
10 Bernasconi, C.F. (1976) Relaxation Kinetics, Academic Press, New York
11 Budesinsky, B. (1969) Talanta 16, 1277–1288
12 Ogan, K. and Simons, E.R. (1979) Anal. Biochem. 96, 70–76
13 Dorogi, P.L., Rabl, C.R. and Neumann, E. (1983) Biochem. Biophys. Res. Commun. 111, 1027–1033
14 Michaylova, V. and Kouleva, N. (1973) Talanta 20, 453–458
15 Michaylova, V. and Kouleva, N. (1974) Talanta 21, 523–532

16 Verkman, A.S., Pandiscio, A.A., Jennings, M. and Solomon, A.K. (1980) Anal. Biochem. 102, 189–195
17 Kendrick, N.C., Atzlaff, R.W.R. and Blaustein, M.P. (1977) Anal. Biochem. 83, 433–450
18 Thomas, M.V. and Gorman, A.L.F. (1978) Biophys. J. 21, 53a
19 Dorogi, P.L. and Neumann, E. (1981) Biophys. Chem. 13, 125–131
20 Budesinsky, B. (1974) Anal. Chim. Acta 171, 343–347
21 Scarpa, A., Brinley, F.J., Jr. and Dubyak, G. (1978) Biochem. 17, 1378–1386
22 Ogawa, Y., Harafuji, H. and Kuregayashi, N. (1980) J. Biochem. 87, 1293–1303
23 Palade, P. and Vergera, J. (1981) in Regulation of Muscle Contraction: Excitation-Contraction Coupling (Grinnell, A.D. and Brazier, M.A.B., eds.), pp. 143–160, Academic Press, New York
24 Dorogi, P.L., Chang, H.W., Moss, K. and Neumann, E. (1981) Biophys. Chem. 14, 91–100
25 Dorogi, P.L., Santarius, U. and Neumann, E. (1982) Anal. Biochem. 124, 27–36
26 Nolte, H.J. and Neumann, E. (1979) Biophys. Chem. 10, 253–260
27 Beeler, T.J., Schibeci, A. and Martonosi, A. (1980) Biochim. Biophys. Acta 629, 317–327
28 Baylor, S.M., Chandler, W.K. and Marshall, M.W. (1979) J. Physiol. 287, 23P–24P
29 Ahmed, Z. and Connor, J.A. (1979) J. Physiol. 286, 56–82